

1 **Alkali metal-resistant mechanism for selective catalytic**
2 **reduction of nitric oxide over V₂O₅/HWO catalysts**

3
4 Running Kang^{a,b}, Junyao He^a, Feng Bin^{a,b*}, Baojuan Dou^c, Qinglan Hao^c,

5 Xiaolin Wei^{a,b}, Kwun Nam Hui^d, Kwan San Hui^{e,**}

6
7 ^a *State Key Laboratory of High-Temperature Gas Dynamics, Institute of Mechanics,*
8 *Chinese Academy of Sciences, Beijing 100190, PR China;*

9 ^b *School of Engineering Science, University of Chinese Academy of Sciences, Beijing*
10 *100049, PR China;*

11 ^c *Tianjin University of Science & Technology, Tianjin 300457, PR China.*

12 ^d *Institute of Applied Physics and Materials Engineering, University of Macau,*
13 *Avenida da Universidade, Taipa, Macau, P.R. China*

14 ^e *School of Engineering, Faculty of Science, University of East Anglia, Norwich*
15 *Research Park, NR4 7TJ, United Kingdom*

16
17 * *Corresponding author. Tel.: +86 10 82544222; fax: +86 10 82544231*

18 ** *Corresponding author. Tel.: +44 01603592582; fax: +44 01603592582*

19 *E-mail address: binfeng@imech.ac.cn (F. Bin); k.hui@uea.ac.uk (K. S. Hui)*
20

21 **Abstract:** A series of V₂O₅/HWO catalysts are prepared by hydrothermal and
22 impregnation methods using different precursors, among which the V₂O₅/HWO-C
23 catalyst exhibited the optimal NH₃-SCR performance. Compared to oxalic acid (O)
24 and water (W), commercial bacterial cellulose (C) as a precursor can firstly achieve a
25 more controllable synthesis to form hexagonal WO₃ (HWO) of V₂O₅/HWO-C catalyst.
26 Various characterization (XRD, N₂-BET, TEM, SEM, XPS, EDX mapping, and

1 NH₃/NO-TPD-MS) indicate that a higher specific surface area, abundant active
2 oxygen and surface acidity result from the V₂O₅/HWO-C catalyst. The reason is that
3 HWO-C has an excellent and smooth rod-shaped morphology, which promotes high
4 dispersion of V₂O₅ on its surface. In situ IR results show that the SCR follows the
5 Langmuir-Hinshelwood (L-H) mechanism, where absorbed NO_x intermediate species
6 are formed on the V₂O₅ and react with the NH₄⁺ and NH₃_{abs} groups of V₂O₅ and HWO.
7 After loading 1.75 wt% K⁺, the obtained K-V₂O₅/HWO-C catalyst exhibits effective
8 resistance to K poisoning and SO₂, and retains 78 % NO_x conversion efficiency at
9 360 °C after 10 h, attributed to the effective capture of K⁺ (1.04 wt%) in HWO-C
10 channels via a new pathway, although approximately 0.71 wt% K⁺ are located on
11 HWO-C external surface with weak bonding to V₂O₅.

12 **Keywords:** Commercial bacterial cellulose; V₂O₅/HWO catalyst; Alkali
13 metal-resistant; Poisoning; SCR reaction

1 **1. Introduction**

2 The selective catalytic reduction (SCR) of NO_x by NH₃ is deemed as an effective
3 strategy for controlling NO_x emissions in flue gas from fuel combustion^[1-4]. The
4 poisoning effect of alkali metals on SCR catalysts, however, is often substantially
5 induced by the combustion of high alkaline solid fuel^{[5][6]}. As the core of this
6 technology for denitration (deNO_x), methods for the synthesis of alkali-resistant
7 catalysts, including those with different active components and diverse preparation
8 methods, have been greatly developed over the past two decades^{[7] [8]}. The
9 deactivation and resistant deactivation mechanisms of catalysts by alkali metals for
10 SCR processing have garnered much attention and have been extensively studied^[9-13].

11 The preparation of vanadium-based SCR catalysts, as a significant design step to
12 realize alkali metal resistance, has both scientific and applied interest. This procedure
13 is crucial for understanding controllable structure synthesis using various precursors
14 to enhance catalytic performance in surficial reactions. Bacterial cellulose as a
15 precursor can be employed instead of the typically used oxalic acid since this
16 inexpensive and green biobased material possesses a three-dimensional network
17 structure and abundant hydroxyl groups that promote nucleation and binding for metal
18 oxide particles. Previously, researchers reported that La₂CuO₄ nanocrystals
19 synthesized by bacterial cellulose nanofibre templates exhibit considerable activity for
20 methanol steam reforming, arising from their unique structure and large specific area
21 ^[14]. Nevertheless, there is limited statistical evidence related to the morphologically
22 controllable synthesis of deNO_x catalysts using different precursors, and the

1 predominant contributor to the enhanced activity has not yet been reported.

2 $V_2O_5-WO_3-TiO_2$ prepared by an oxalic acid precursor, as a traditional and
3 commercial deNO_x catalyst, is commonly employed owing to its excellent catalytic
4 properties [15][16][17]. Lian et al reported that the V_2O_5/TiO_2 catalyst with high rutile
5 phase content exhibited superior NH₃-SCR catalytic performance [18]. Unfortunately,
6 the catalyst is easily deactivated in flue gas containing alkali metals. Deng et al. [19]
7 pointed out that upon the addition of various alkali metals, the activity of the
8 $V_2O_5-WO_3-TiO_2$ catalyst was greatly inhibited by K and Na (in decreasing order) due
9 to the decreasing specific surface area and the masking of V_2O_5 . Kong et al suggested
10 that the deactivation rate of potassium-poisoned catalysts follows $KCl > K_2O > K_2SO_4$
11 in the SCR reaction over the $V_2O_5-WO_3-TiO_2$ catalyst [20]. Although supported
12 $V_2O_5-WO_3/TiO_2$ catalysts have not been extensively examined for the interaction
13 between TiO_2 , V_2O_5 and alkali metals, some publications imply that the nature of the
14 supported vanadium oxide sites depends on the specific precursors and preparation
15 methods [21-24], but these claims were not given by supporting information. Recently,
16 several successful attempts have been made to improve the alkali metal-resistant
17 performance of vanadium oxide catalysts [25]. According to Hu et al. and Huang et al.
18 [24][26], MnO_2 and WO_3 prepared by oxalic acid as precursors can effectively trap
19 alkali metal ions and prevent V_2O_5 poisoning during SCR due to the structure of
20 MnO_2 and WO_3 . Further, the Zheng et al. proposed self-protect mechanism via
21 alkali-trapping of HWO rather than including alkali-blocking of V_2O_5 in the SCR
22 process over V_2O_5/HWO catalyst using oxalic acid precursor [27]. Despite previous

1 studies concerning deactivation and resistant deactivation models of alkali metals in
2 the SCR reaction, the exact distribution of alkali metal species with quantitative or
3 semi quantitative analysis on the catalyst leading to the alkali metal-resistant
4 mechanism remains unclear.

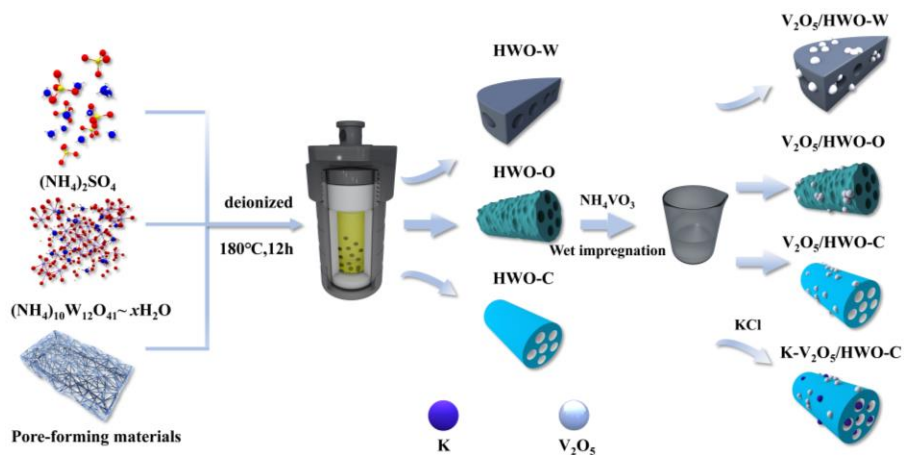
5 In this investigation, a series of V₂O₅/HWO catalysts are prepared by three
6 different precursors, including commercial bacterial cellulose, oxalic acid and water,
7 to study the interactions among the morphological characteristics and the catalytic
8 activity in the SCR reaction. In particular, the alkali metal-resistant pathways for the
9 distribution of alkali metal ions (K⁺) on the catalyst and V₂O₅/HWO-C were proposed
10 in detail via X-ray diffraction (XRD), transmission electron microscopy (TEM),
11 energy-dispersive X-ray spectroscopy (EDX) mapping, X-ray photoelectron
12 spectroscopy (XPS) and in situ infrared (in situ IR) analysis. The results obtained will
13 provide new insights into the design of advanced catalysts and the corresponding
14 alkali metal-resistant mechanisms for SCR reactions.

15 **2. Experimental specifications**

16 ***2.1 Catalyst preparation***

17 To investigate the relationship between the porous structure and activity, HWO
18 was prepared by a hydrothermal method using different pore-forming agents,
19 including commercial bacterial cellulose (C), oxalic acid (O) and water (W). The
20 (NH₄)₁₀W₁₂O₄₁~xH₂O (2.13 g), (NH₄)₂SO₄ (8.32 g) and pore-forming materials (2.10
21 g) were dissolved in deionized H₂O (80 mL). The homogeneous solution was kept at
22 180 °C for 12 h in an autoclave (200 mL) and then washed with deionized H₂O,

1 followed by drying at 120 °C. The theoretical support content of V_2O_5 is 10% in the
 2 all catalysts. The obtained catalysts were denoted as HWO-C, HWO-O and HWO-W.
 3 The V_2O_5 /HWO catalysts were synthesized by wet impregnation of the various HWO
 4 with NH_4VO_3 solutions. The resulting solutions were stirred and evaporated at 80 °C
 5 for 0.5 h, and then they were calcined at 400 °C for 4 h to obtain V_2O_5 /HWO-C,
 6 V_2O_5 /HWO-O and V_2O_5 /HWO-W catalysts. The K in gas phase is always absorbed
 7 and migrated on the catalyst in the flue gas. Therefore, considering that the
 8 deactivation of the catalyst by alkali metals in off-gas is a long-term process, the
 9 alkali resistance of the samples was simulated by immersing method and to realize
 10 extreme condition of K loading and poisoning. To study the actual deactivation as
 11 well as the capture of K^+ via the catalyst surface morphology and channels for the
 12 SCR reaction, a KCl (0.03 g) aqueous solution was loaded with stirring onto the
 13 V_2O_5 /HWO-C (1 g) catalyst and dried at 120 °C for 4 h to obtain K- V_2O_5 /HWO-C.
 14 The schematic diagram describing the catalysts preparation is shown in Fig. 1. The
 15 metal content in the catalysts was detected by X-ray fluorescence (XRF) and is shown
 16 in Table 1.



17 **Fig.1.** Schematic diagram of the catalysts preparation.

1 *2.2 Characterization*

2 The elemental composition of the catalysts was obtained by XRF with a Power
3 4200 scanning XRF spectrometer. The textural properties were investigated by N₂
4 adsorption-desorption (N₂-Brunauer, Emmett and Teller, N₂-BET) at the liquid
5 nitrogen temperature using a 16 Autosorb-Iq-MP instrument (Quantachrome). XRD
6 patterns were measured by an XD-3-automatic (PERSEE) equipped with a Cu K α
7 radiation source (λ = 0.1541 nm). Rietveld refinement analyses of the XRD data
8 profiles were subsequently performed by using TOPAS Academic and Fullprof
9 software package. The morphology and distribution of surface elements were
10 determined by TEM (JEM 2100F, Oxford) equipped with EDX mapping (Tecnai G²
11 F20, Oxford). Temperature-programmed reduction (H₂-TPR) was conducted on a
12 TP5080B chemisorption analyzer with approximately 50 mg of each example. Each
13 sample was pretreated at 300 °C for 0.5 h in a flow of N₂ (50 mL/min). The
14 temperature was increased from room temperature to 900 °C at a heating rate of
15 10 °C/min in a flow of a H₂ (30 mL/min), and the H₂ consumption was recorded
16 continuously by the TCD detector. Temperature-programmed NH₃ desorption
17 (NH₃-TPD-TCD) experiments were performed using a TP5080B chemisorption
18 analyser with 5 vol% NH₃/Ar (50 mL/min) at a heating rate of 10 °C/min from 100 °C
19 to 800 °C. The absorbed gases were passed through the samples for 1 h at 100 °C and
20 started desorption to maintain stable NH₃ absorption and avoid the signal interference.
21 Temperature-programmed desorption of NO, and NH₃ (NO- and NH₃-TPD-MS) was
22 also conducted by same analyzer, monitored by an online quadrupole mass

1 spectrometer (MS, Pfeiffer Omnistar™). After being pretreated at 300 °C under
2 flowing helium (50 ml/min) for 1 h, the powder sample (20 mg) was cooled to 50 °C
3 and then adsorbed to saturation by 5 vol% NO/He, or 5 vol% NH₃/He for 0.5 h. The
4 desorption signals were recorded from 50 °C to 1000 °C at an increasing rate of
5 10 °C/min. For the chemical states of surface elements, XPS was carried out with a
6 Kratos Axis Ultra DLD spectrometer. The binding energy of surface elements was
7 calibrated with C1s (284.8 eV) peak. In situ IR spectroscopy was recorded with a
8 Bruker Tensor 27 spectrophotometer with a self-designed magnetically driven
9 transmission cell. Prior to obtaining each IR spectrum, the sample (20 mg) was
10 pretreated under N₂ flow with 100 mL/min at 400 °C to remove adsorbed impurities.
11 The spectra were recorded by accumulating 32 scans at a heating rate of 10 °C/min to
12 500 °C after the absorption of reactants for 0.5 h.

13 ***2.3 Catalytic activity testing***

14 The SCR activity test was evaluated under atmospheric pressure in a fixed-bed
15 quartz tube reactor (i.d.=4 mm). The catalyst (200 mg, 0.1-0.15 mm) was charged for
16 each test. The feed gases contained 300 ppm NO, 300 ppm NH₃, 5 vol.% O₂ and N₂ as
17 the balance gas with a total flow rate of 200 mL/min, corresponding to a gas hourly
18 space velocity (GHSV) of 170,000 h⁻¹. Temperature-programmed catalytic reduction
19 of NO was performed under heating (10 °C/min) from room temperature to 400 °C,
20 and a K-type thermocouple was positioned between the reactor and oven wall to
21 monitor the oven temperature. The concentrations of NO, NH₃, SO₂ and O₂ were
22 measured by an online multicomponent analyser (Gasboard-300UV for NO (±2%FS))

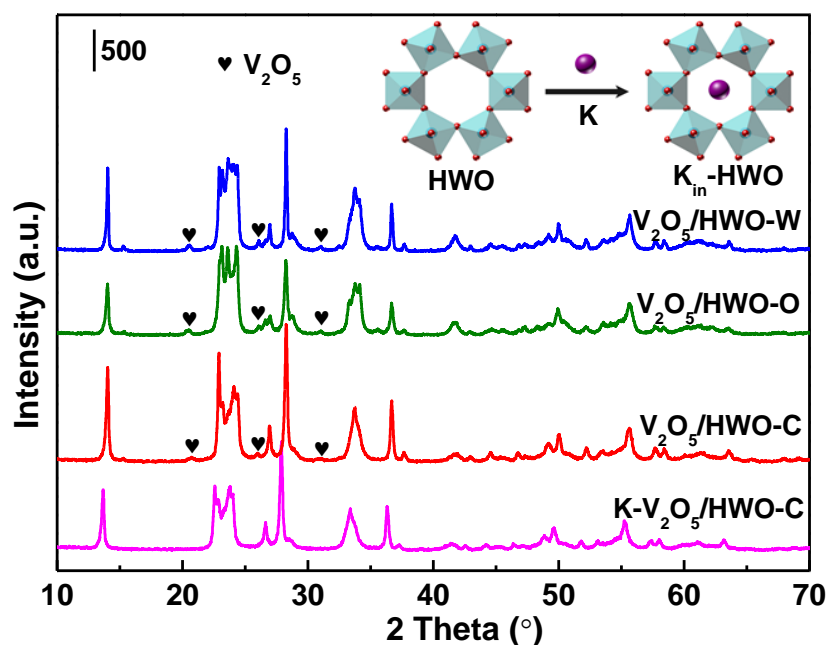
1 /NH₃ ($\pm 4\%$ FS) /O₂ ($\pm 3\%$ FS), and Gasboard-300plus for SO₂ ($\pm 2\%$ FS), Hubei
2 Cubic-Ruiyi Instrument Co., Ltd.). Good reproducibility of catalysts was found for
3 each SCR experiment at three times.

4 **3. Results and discussion**

5 *3.1 Structure, morphology and occurrence state*

6 Figure 2 displays the XRD patterns of the V₂O₅/HWO-W, V₂O₅/HWO-O,
7 V₂O₅/HWO-C and K-V₂O₅/HWO-C catalysts. Apart from the strong characteristic
8 diffraction peaks of hexagonal WO₃ for all the catalysts (PDF#75-2187), weak
9 diffraction peaks assigned to V₂O₅ crystals (PDF#85-0601) can be observed in the
10 spectra of V₂O₅/HWO-W, V₂O₅/HWO-O and V₂O₅/HWO-C. The size of HWO
11 channels is not large enough to accommodate V₂O₅ particles^[26], so that V₂O₅ is
12 dispersed on the external surface of HWO rather than being introduced into HWO
13 channels. The only weak peaks of V₂O₅ are detected on the V₂O₅/HWO-W,
14 V₂O₅/HWO-O and V₂O₅/HWO-C in the Fig.2, indicating that the most vanadium
15 species are well dispersed and correspondingly, a little part of vanadium species are
16 formed as crystalline on the catalysts. Furthermore, Compared with V₂O₅/HWO-W
17 and V₂O₅/HWO-O, V₂O₅/HWO-C shows relative highly dispersed states of V₂O₅ on
18 the surface, according to the existence of much too weak peaks of V₂O₅ at 20.7° (001
19 plane), 25.9° (101 plane) and 31° (031 plane). After K⁺ was loaded, the peak of V₂O₅
20 crystallites became weaker and less obvious, which means that the active component
21 of vanadium might be covered by some K⁺ on the catalyst surface ^[28]. Surprisingly,
22 the shift of the diffraction peaks of HWO towards lower 2 θ values for

1 K-V₂O₅/HWO-C reveals that most K⁺ ions are probably inserted into the HWO
 2 channels to cause a bigger lattice constant. The strength of HWO slightly decreases
 3 could be assigned to the some K⁺ covered on the catalyst surface. A structural model
 4 of the local situation of K⁺ is shown in the inset of Fig. 2.



5

6

Fig. 2. XRD patterns of the catalysts.

7

8

9

10

11

12

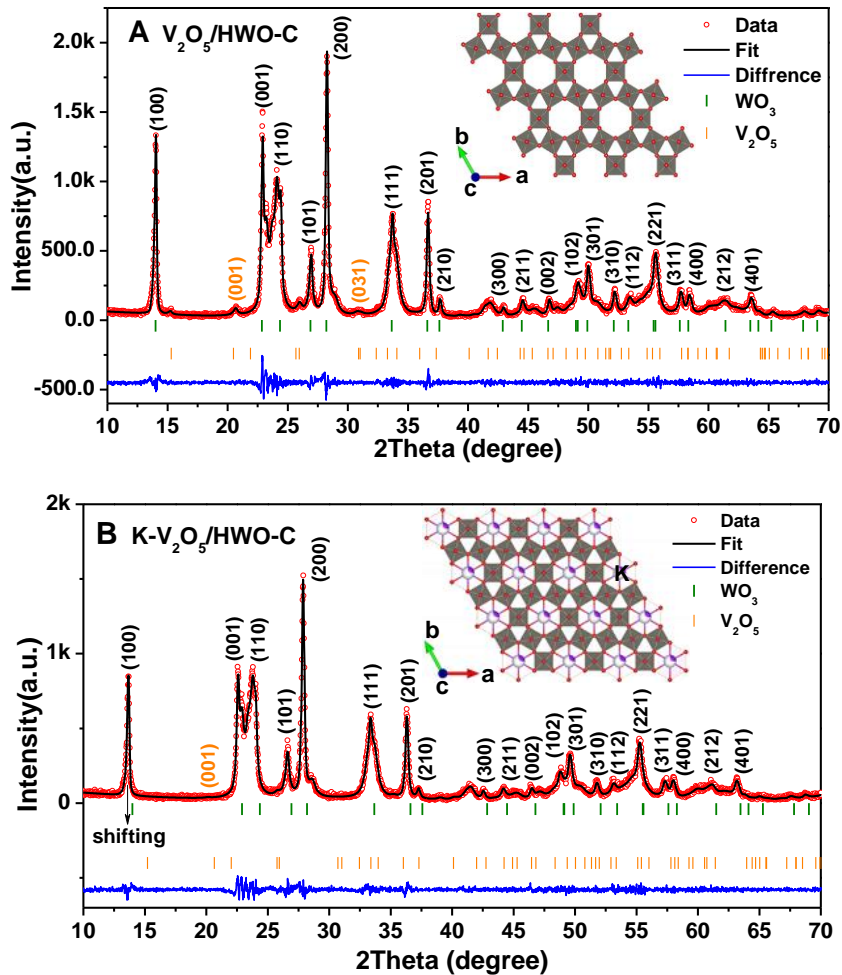
13

14

15

To further confirm the K⁺ position, the corresponding Rietveld XRD refinements of V₂O₅/HWO-C and K-V₂O₅/HWO-C catalysts are shown in Fig.3. All the Bragg reflections of the K-V₂O₅/HWO-C transfer to lower angles, in comparison with the V₂O₅/HWO-C. Then the calculated lattice constants of HWO (7.2993Å × 7.2993Å × 3.8872Å) on the V₂O₅/HWO-C exhibit an expansion of a and b axis and a contraction of c axis after K⁺ insertion into the HWO tunnels (7.3088Å × 7.3088Å × 3.8807Å) over K-V₂O₅/HWO-C (Table S1). The Rietveld refinement analyses show that the K⁺ occupies exactly at the Wyckoff 1a site or the (0,0,0) site and the occupation 0.25 (Table S2), indicating that the K⁺ ions are coordinated to six oxygen atoms (K-O) in

1 the channels with a mean K-O bond length of $\sim 2.68 \text{ \AA}$ [26]. Based on the typical Space
 2 group of HWO (P6/mmm), a structural model of the local region of K^+ is carried out
 3 in the inset of Fig. 3.



4

5

6 **Fig.3.** XRD patterns (red lines) and corresponding Rietveld refinements (black lines) of the (A)
 7 $\text{V}_2\text{O}_5/\text{HWO-C}$ and (B) $\text{K-V}_2\text{O}_5/\text{HWO-C}$. The green lines are the differential XRD pattern of the
 8 catalysts. The short vertical lines below the XRD patterns are assigned to the peak positions of all
 9 the possible Bragg reflections.

10 The N_2 adsorption-desorption isotherms are analysed to study the difference in
 11 specific surface area (SSA), pore volume and pore size over various catalysts, as
 12 shown in Fig. 4. All the catalysts show type IV isotherms with a H3-type hysteresis
 13 loop, indicating that a large number of mesopores are formed in the catalysts. Due to

1 the abundant network structure of commercial bacterial cellulose, $V_2O_5/HWO-C$
2 shows a higher SSA ($11.85 \text{ m}^2/\text{g}$) than $V_2O_5/HWO-W$ ($4.88 \text{ m}^2/\text{g}$) and $V_2O_5/HWO-O$
3 ($8.92 \text{ m}^2/\text{g}$) and, therefore, promotes the dispersion of V_2O_5 on the HWO surface.
4 Particularly, the pores (Fig. 4b) show an exclusive region with a size less than 5 nm
5 for $V_2O_5/HWO-C$ by using bacterial cellulose as pore forming materials, favouring
6 the formation of abundant channels for HWO and the interaction between many more
7 V_2O_5 active sites and the HWO support, thus improving the catalytic performance. It
8 has been reported that the small size ($<5\text{nm}$) among the supported catalyst promotes
9 the formation of coordinated atoms with higher chemical activity^[29]. The pore volume
10 of $V_2O_5/HWO-C$ ($0.033 \text{ cm}^3/\text{g}$) is approximately equal to that of $K-V_2O_5/HWO-C$
11 ($0.031 \text{ cm}^3/\text{g}$) since some K^+ is located in the channels of the $K-V_2O_5/HWO-C$
12 catalyst via HWO trapping^[30]. There are visible differences between $V_2O_5/HWO-C$
13 and $K-V_2O_5/HWO-C$ for both SSA and mean pore size. The $V_2O_5/HWO-C$ shows a
14 bigger SSA and a lower mean pore size than that of $K-V_2O_5/HWO-C$, attributed to
15 partially K^+ leads to block the micropores entrance, and agglomeration between some
16 K^+ and vanadium oxides causes the SSA decreasing and means pore size of
17 accumulation pores increasing. This finding indicates that the other K^+ ions may
18 diffuse onto the surface of the catalyst or block the entrance of HWO channels.

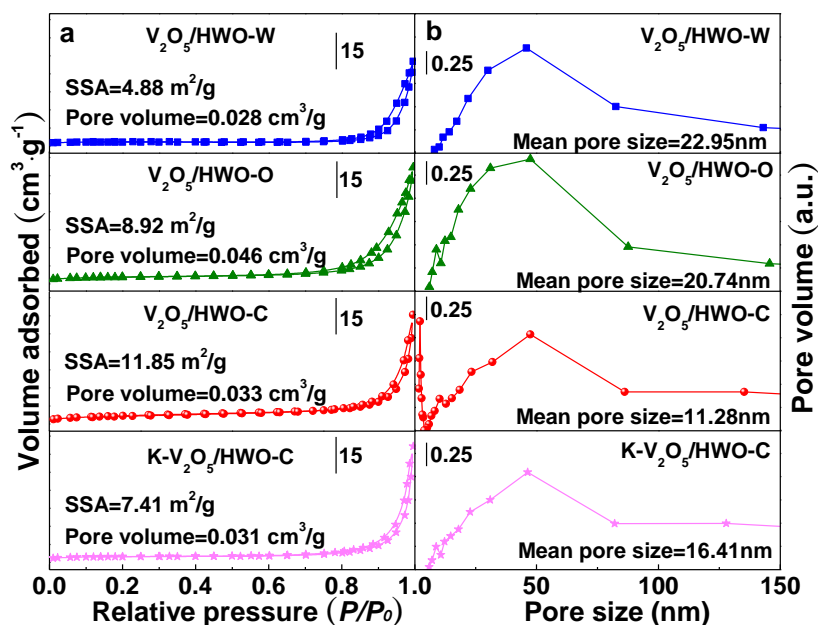
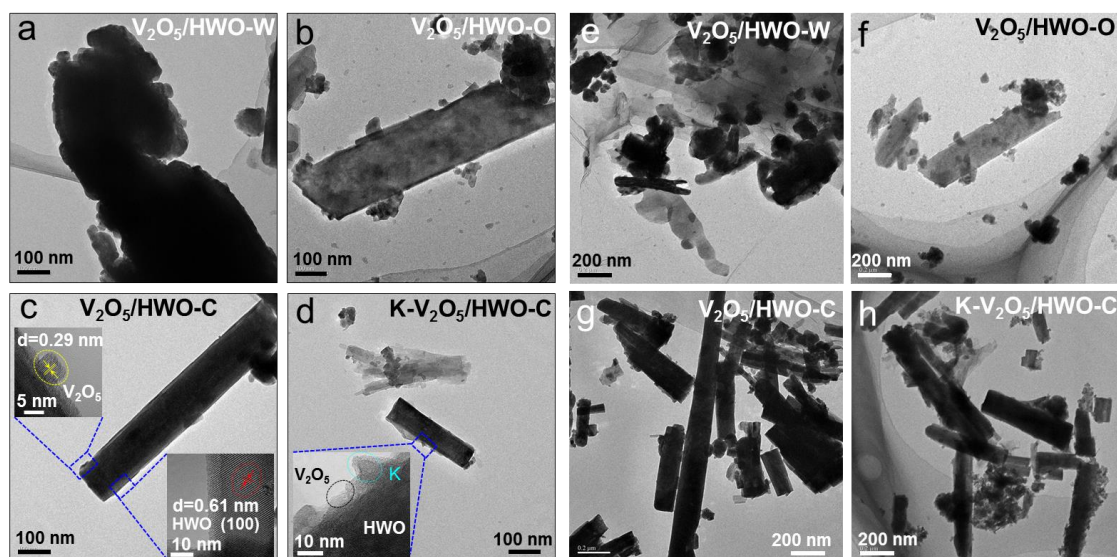


Fig. 4. N₂ adsorption-desorption isotherms (a) and pore size distribution (b) of catalysts.

Representative TEM images of the catalysts are presented in Fig. 5. Among all tested catalysts, V₂O₅/HWO-C (Fig. 5c and 5g) exhibits the best and smoothest rod-shaped morphology of HWO and a good dispersion of V₂O₅ on the surface. Commercial bacterial cellulose possesses an ultrafine three-dimensional network structure and unique properties including high crystallinity, good tensile strength, and mouldability. Therefore, the cellulose here not only promotes controllable synthesis to form a catalyst with a regular morphology but also possesses a high surface area for dispersing more metal ions, which is in agreement with the XRD and N₂-BET results. High-resolution TEM (HR-TEM) is further performed on V₂O₅/HWO-C (Fig. 5c), where a representative individual HWO rod with the side line parallel to the (100) plane is found by the fringe distance of 0.61 nm. Crystalline V₂O₅ is observed on the surface of HWO by measuring the D spacing at d=0.29 nm. Typical morphologies with broader scales are also displayed in Fig. 5e-h. The loading of K⁺ results in no visible change in the rod-shaped morphology (Fig. 5d), but some K⁺ ions are found on

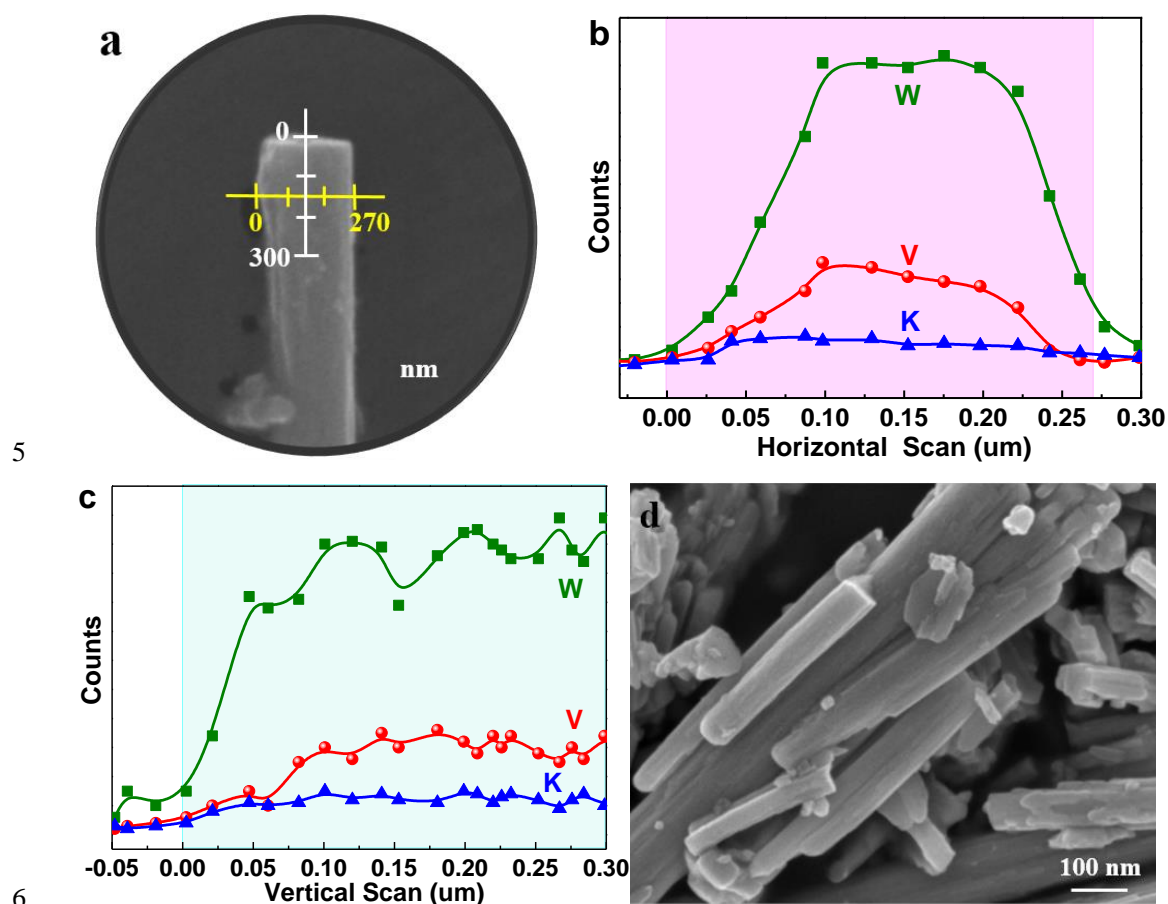
1 the surface of K-V₂O₅/HWO-C. Although the HWO channels synthesized by many
 2 precursors would be about 0.54 nm and V₂O₅ nanoparticles will not be captured [31].
 3 The size of the HWO channels is ~0.54 nm, which is appropriate for accommodating
 4 metal ions with ionic radii less than 0.17 nm [32], thus easily capturing K⁺ (0.13 nm) in
 5 the many easily formed HWO channels rather than capturing V₂O₅ nanoparticles for
 6 the K-V₂O₅/HWO-C. According to the results above, there are two locations for K⁺
 7 ions: i) on the HWO external surface and ii) inside the HWO channels in a stable
 8 state.



9
10 **Fig. 5.** TEM images of catalysts.

11 The distribution of elements in the cross-section channel of K-V₂O₅/HWO-C
 12 catalyst have been given in Fig.6 (a), (b) and (c). It is clear that the vanadium and part
 13 potassium species are detected on the HWO surface and the presence of the isolated
 14 individual potassium atoms. Combined with the Rietveld refinements and TEM
 15 results, these results are further confirmed thus most potassium ions are effectively
 16 captured in HWO-C channels through an ions exchange path in HWO-C channels.

1 The hexagonal morphology of HWO-C in V_2O_5 /HWO-C catalyst has been also well
 2 characterized by SEM, as shown in Fig. 6(d). It can be found that the controllable
 3 synthesis of catalytic hexagonal morphology was achieved successfully for the
 4 V_2O_5 /HWO-C catalyst.



5
 6
 7 **Fig. 6.** (a) TEM images with line-scanned EDX spectra of the K- V_2O_5 /HWO-C, (b)
 8 horizontal line-scanned, (c) vertical line-scanned, (d) SEM image of V_2O_5 /HWO-C

10 *3.2 Chemical states, distribution of elements and acidity*

11 The chemical states and surficial element compositions of the catalysts are
 12 investigated by XPS analysis. The V 2p spectra of the catalysts (Fig. 7a) show three
 13 main peaks for V^{5+} (517.1 eV), V^{4+} (516.3 eV) and V^{3+} (515.3 eV) [33]. The
 14 semiquantitative data, as listed in Table 1, give $(V^{5+}+V^{4+}) / V_{total}$ ratios of 0.937 for

1 $V_2O_5/HWO-C$, 0.971 for $V_2O_5/HWO-O$, 0.980 for $V_2O_5/HWO-W$ and 0.952 for
2 $K-V_2O_5/HWO-C$. After loading K^+ ions on the $V_2O_5/HWO-C$ catalyst, the ratio of the
3 lattice oxygen (O_L^{2-}) in the $K-V_2O_5/HWO-C$ increases, and occurring the slightly
4 change of vanadium chemical valence during the bond between V_2O_5 and partial K on
5 the catalyst surface, hence the $(V^{5+}+V^{4+})/V_{total}$ ratios of $V_2O_5/HWO-C$ (0.937) is
6 lower than $K-V_2O_5/HWO-C$ (0.952). The W 4f spectra of the catalysts (Fig. 7b) are
7 deconvoluted into $4f_{5/2}$ and $4f_{7/2}$ spin-orbit components [34][35]. The presence of W^{6+} in
8 the catalysts favours the formation of a strong carrier-metal interaction via electronic
9 transitions between W^{6+} and V^{n+} [36][37]. The O 1s curve (Fig. 7c) is fitted to two peaks
10 corresponding to surface-adsorbed oxygen (O_a , 531.6 eV) and lattice oxygen (O_L ,
11 530.5 eV)[38, 39]. The peak of hydroxyl species is too low to fit accurately at ~ 530.8 eV
12 due to a large peak at 530.5 eV for lattice oxygen in the catalysts. It was reported that
13 O_a is the most active oxygen species that plays a crucial role in the SCR reaction due
14 to its higher mobility on the catalyst surface than the inactive O_L [33]. Herein, O_a ratios
15 are calculated by $O_a/(O_a+O_L)$ and decrease in the following order (Fig. 7c):
16 $V_2O_5/HWO-C$ (31.2 %) > $K-V_2O_5/HWO-C$ (30.6 %) > $V_2O_5/HWO-O$ (25.5 %) >
17 $V_2O_5/HWO-W$ (22.5 %). The high O_a ratios of $V_2O_5/HWO-C$ and $K-V_2O_5/HWO-C$
18 should be related to the abundant oxygen ions in the commercial bacterial cellulose,
19 which promotes contact with more metal ions in the catalysts. The K 2p spectra of
20 $K-V_2O_5/HWO-C$ were also obtained (as shown in the Fig. S1), verifying that some K^+
21 ions exist on the catalyst surface.

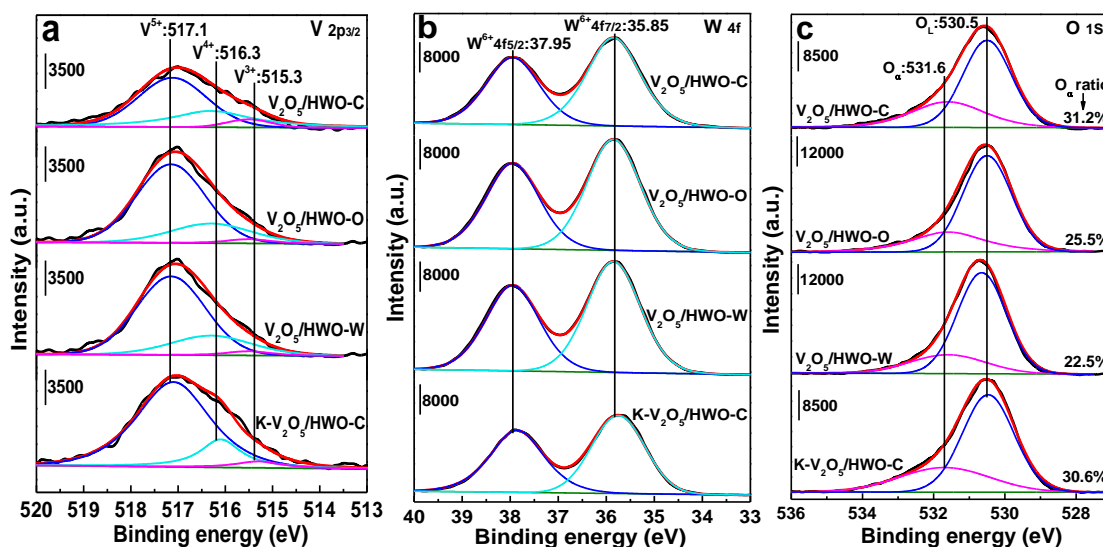


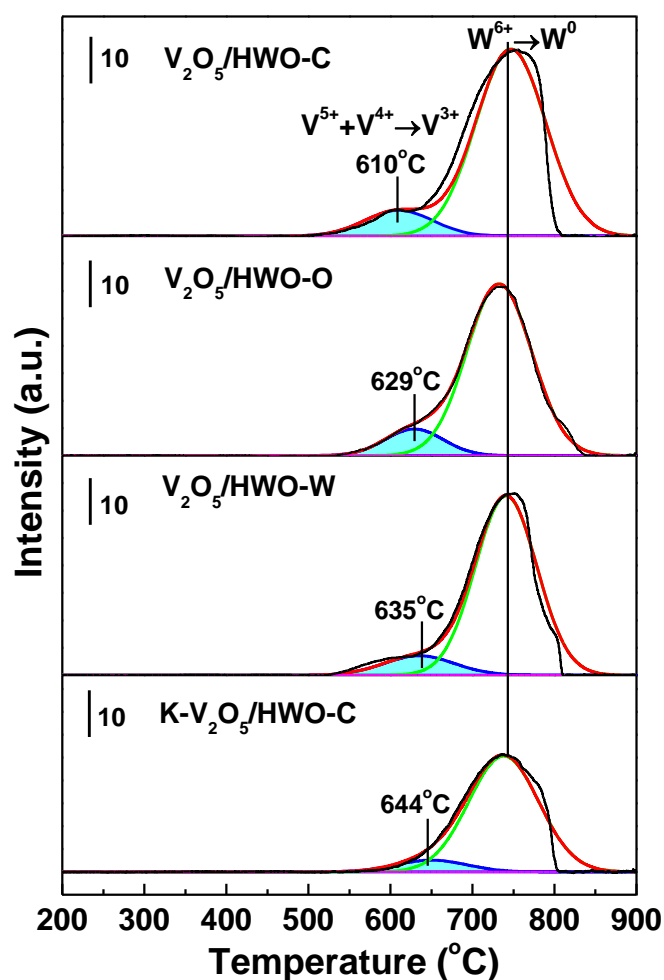
Fig. 7. XPS spectra of (a) V 2p, (b) W 4f and (c) O 1s over the catalysts.

Table 1 The element content, the atomic content and the number of absorbed NH₃ on acid sites on the surface of the catalysts.

Samples	V ₂ O ₅ (%)	WO ₃ (%)	K/K ₂ O (wt%)	(V ⁵⁺ +V ⁴⁺)/V _{total}
V ₂ O ₅ /HWO-W	10.05	89.95	--	0.980
V ₂ O ₅ /HWO-O	10.02	89.98	--	0.971
V ₂ O ₅ /HWO-C	9.87	90.13	--	0.937
K-V ₂ O ₅ /HWO-C	9.74	88.51	1.75	0.952

The redox ability of vanadium and tungsten species with different precursors and alkali metal of catalysts were investigated with H₂-TPR analysis, as shown in Fig. 8. The reduction peaks located at 610-644 °C and 730-750 °C are ascribed to reduction of V⁵⁺/V⁴⁺ → V³⁺ and W⁶⁺ → W⁰, respectively^[40]. The dispersed vanadium is considered as a key catalytic cycle for the SCR reaction due to the peak position of W species showed no obvious change in the catalysts although the content of W is far more than that of V. Compared with the peaks of vanadium on the V₂O₅/HWO-O (629 °C) and V₂O₅/HWO-W (635 °C), the V₂O₅/HWO-C shifts to lower temperature (610 °C), indicating that the well dispersed vanadium species are easily reduced and

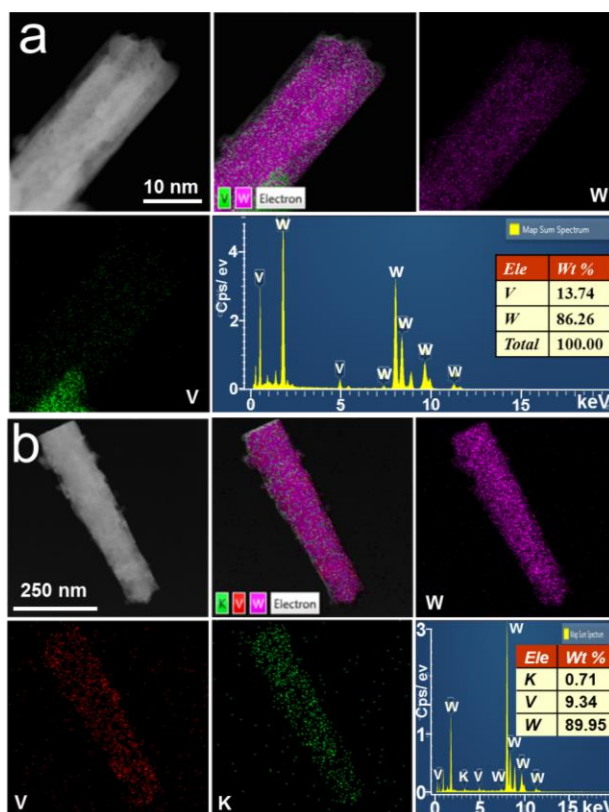
1 promote the activity of $V_2O_5/HWO-C$. This is consistent with the XRD, TEM, O_a of
 2 XPS and SCR activity results. After loading K^+ on the $V_2O_5/HWO-C$, the reduction
 3 peak of V species of $K-V_2O_5/HWO-C$ shifts to higher temperatures (644 °C),
 4 attributed to partial K^+ bonds and weakens the oxidation activity of V species [41].
 5 Further the peak intensity of W species for $K-V_2O_5/HWO-C$ become lower than that
 6 of $V_2O_5/HWO-C$, suggesting that the captured K^+ in HWO channel has a stronger
 7 interaction with oxygen in tungsten oxides.



8
 9 **Fig. 8.** H_2 -TPR profiles of the catalysts.

10 The potassium element loaded on the whole regular $K-V_2O_5/HWO-C$ rod would
 11 have an effect on the SCR activity. The TEM images, corresponding EDX maps and

1 semiquantitative analysis of $V_2O_5/HWO-C$ and $K-V_2O_5/HWO-C$ are shown in Fig. 9,
2 which illustrate the spatial distribution and high dispersion of vanadium and
3 potassium on the catalyst surface. The vanadium and potassium species are well
4 dispersed on the HWO external surface. There are three possible locations for K^+ ions:
5 i) on the HWO external surface not in conjunction with V_2O_5 , ii) on the HWO
6 external surface in conjunction with V_2O_5 , and iii) at the entrance into the HWO
7 channels. Based on the N_2 -BET results, the mean pore size of $K-V_2O_5/HWO-C$ (16.31
8 nm) is higher than that of $V_2O_5/HWO-C$ (11.28 nm). The increase in the mean pore
9 size is responsible for the partial number of K^+ ions making contact with V_2O_5 to form
10 relatively large particles on the catalyst surface, possibly resulting in a decrease in the
11 catalyst activity in the SCR reaction, which can be confirmed by the SCR activity in
12 Fig. 12. Therefore, the locations of K^+ should be determined in the last two forms as
13 discussed above. The obtained contents of tungsten and vanadium elements are also
14 similar to the XRF results for typical $K-V_2O_5/HWO-C$ rod (big scale at 250 nm).
15 Hence the EDX shows that the content of K^+ is 0.71 wt% on the whole surface of
16 HWO (Fig. 9b) tested, whereas the total content of K^+ on $K-V_2O_5/HWO-C$ is 1.75
17 wt% via XRF analysis (Table 1). To sum up, 0.71 wt% K^+ has been located on the
18 HWO-C external surface and 1.04 wt% K^+ has entered into the HWO-C channels
19 according to the semiquantitative analysis.



1

2 **Fig. 9.** TEM images, EDX mapping and spectrum of the (a) V₂O₅/HWO-C and (b)

3

K-V₂O₅/HWO-C catalysts.

4

5

6

7

8

9

10

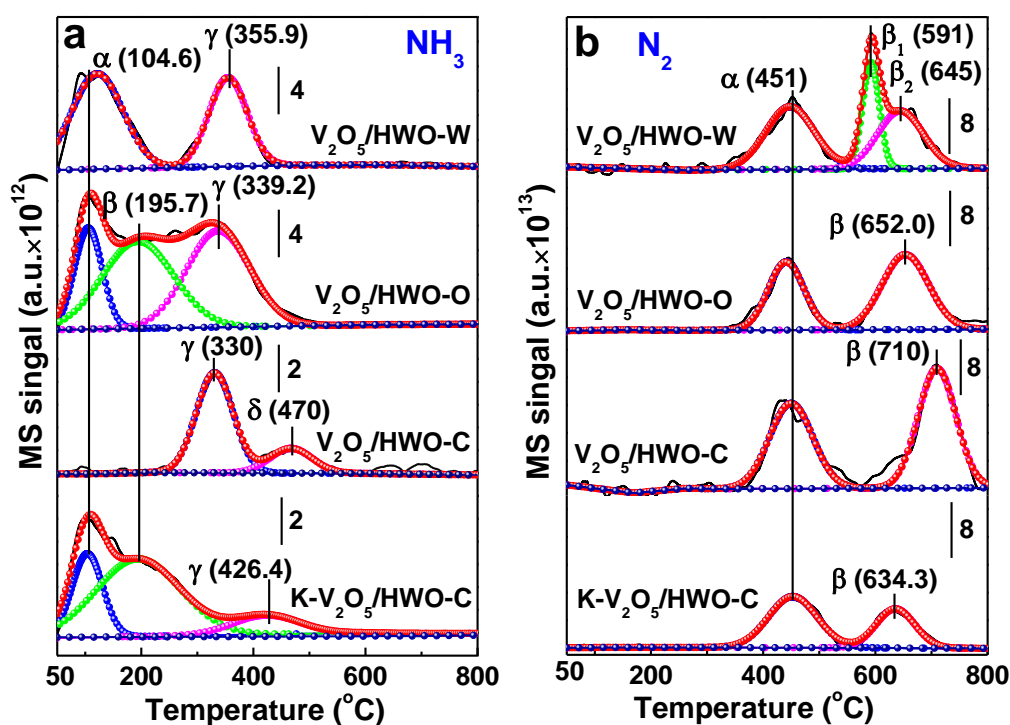
11

12

13

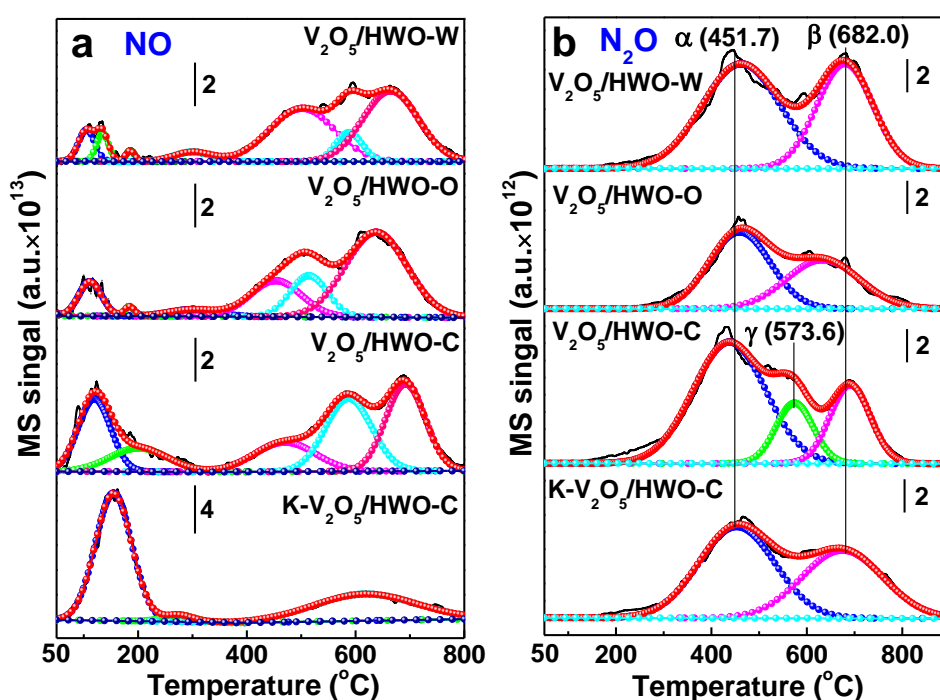
As a traditional acidity analysis, the desorption temperature in the NH₃-TPD-TCD experiment is always to start about 100 °C to avoid the signal interference, as shown in Fig S3. It can be seen that the peaks located < 220 °C and > 300 °C are assigned to the weak and strong adsorbed NH₃ on acid sites, respectively. However the TCD signal can't represent and clarify all gases signals during NH₃ desorption process. Furthermore, in order to measure different gases in the NH₃-TPD process exactly, the online NH₃-TPD-MS is carried out to record the desorption process from the 50 °C to 800 °C. The NH₃-TPD-MS results could be more accurate to distinguish the acid strength and avoid interference caused by the signal peaks of other substances. The NH₃ signals of catalysts are monitored by the mass

1 spectrometer (Fig. 10a). Correspondingly, the N₂ signal is detected synchronously to
 2 evidence that the NH₃ adsorbed on acid sites is thermally desorbed to yield N₂ (Fig.
 3 10b). The large NH₃ chemical desorption curves around 200 °C is contributed to
 4 weakly bond NH₃ on the acid sites (Lewis acid) for the catalysts. The two typical
 5 medium-temperature desorption peaks of NH₃ (γ and δ) and two remarkable peaks of
 6 N₂ (α and β) are found on the V₂O₅/HWO-C catalyst, indicating that the NH₃ bond to
 7 strong acid sites (Brønsted acid) on V₂O₅/HWO-C is more easily activated and
 8 thermally desorbed to yield N₂ release, and closely attributable to the selective
 9 reduction of NO for SCR reaction. Our previous work found that the Brønsted acid
 10 sites not only bind and disperse transition metal ions but also absorb and activate
 11 ammonia^[42,43]. Hence, the role is contradictory because metal ions well dispersed here
 12 are unable to bind a significant amount of physisorbed NH₃ on the V₂O₅/HWO-C.



13
 14 **Fig. 10.** NH₃-TPD-MS (a) NH₃ and (b) N₂ profiles of the catalysts.

1 The NO desorption analysis is also carried out to detected the NO and N₂O
 2 signals in Fig.11a and 11b during NO-TPD, assigned to the key step of SCR reaction
 3 [44]. The desorption peak of NO centered in the <200 °C is attributed to the physical
 4 desorption of NO bounded to amorphous clusters and well dispersed V₂O₅ oxides,
 5 easily absorbed on the some K⁺ of the K-V₂O₅/HWO-C surface (Fig.11a), and another
 6 peak at >200 °C corresponds to the chemical desorption of NO strongly bounded to
 7 bulk V₂O₅ oxides. The N₂O curves is measured synchronously at 180-800 °C since
 8 the NO is tend to be adsorbed on metal sites, and two N-O bonds are activated to
 9 convert into N₂O at elevated temperatures. The remarkable desorption peak area of
 10 N₂O is observed (Fig.11b) at low temperature over V₂O₅/HWO-C, supporting that the
 11 relatively weak bond strength between well dispersed vanadium species and NO
 12 would facilitate the selective reduction of NO with NH₃, which is similar to the results
 13 of the other literatures^[45, 46].

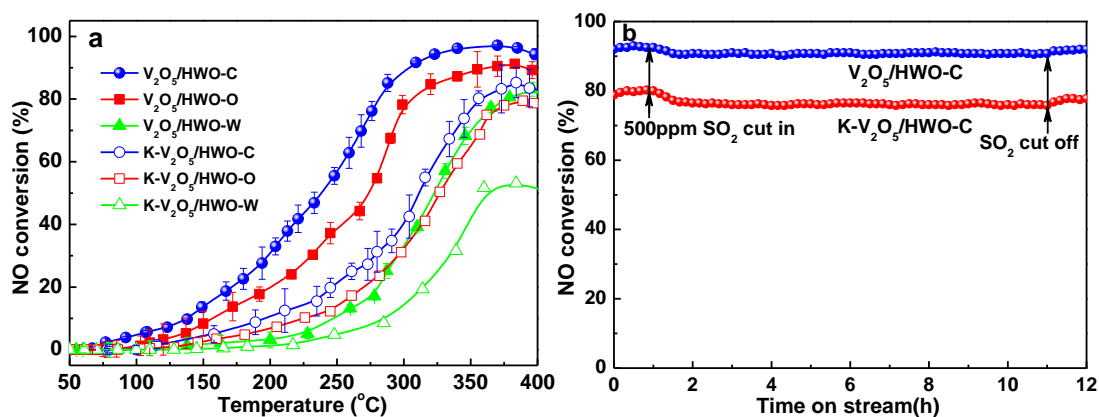


14 **Fig. 11.** NO-TPD-MS (a) NO and (b) N₂O profiles of the catalysts.
 15

1 3.3 SCR activity and resistance to K poisoning

2 Figure 12 displays the SCR activity and duration tests for the catalysts to show
3 the catalytic activity and alkali resistance capacity. The $V_2O_5/HWO-C$ catalyst
4 exhibits a higher activity than that of $V_2O_5/HWO-W$ and $V_2O_5/HWO-O$, reaching a
5 maximum NO conversion of 97 % at 360 °C and > 90 % NO conversion within the
6 wide temperature range of 300-400 °C (Fig. 12a). The excellent activity obtained for
7 $V_2O_5/HWO-C$ can be attributed to the good dispersion of V_2O_5 on the smooth
8 rod-shaped morphology of HWO and the abundant number of active oxygen atoms
9 and acid sites on the catalyst surface, as proven by the XRD, TEM, H_2 -TPR and XPS
10 results. After being subjected to a K^+ load, $K-V_2O_5/HWO-C$ exhibits acceptable alkali
11 resistance, with the highest NO conversion reaching 83 % at 360 °C among all the
12 catalysts tested. The good N_2 selectivity below the 400 °C is also obtained in the
13 Fig.S4. The SCR activity and alkali resistance compared to the reported catalysts ^[26]
14 ^[27] ^[41] ^[47] ^[28] are shown in Table 2. It was reported that the presence of SO_2 may have
15 a negative effect on the alkali resistance of V_2O_5 -based catalysts ^[41] ^[49] ^[50]. Hence the
16 influence of SO_2 on SCR stability was tested over the $V_2O_5/HWO-C$ and
17 $K-V_2O_5/HWO-C$, with the results shown in Fig.12b. When 500 ppm (1400 mg/m³) of
18 SO_2 was introduced, the NO conversion for $V_2O_5/HWO-C$ and $K-V_2O_5/HWO-C$
19 slightly decreased from 93% to 91% and from 80% to 76% respectively, and maintain
20 at such a conversion level for approximate 10 hours, which indicate that slight
21 interactions were occurred between alkalis and SO_2 in the SCR process. The activity
22 of $V_2O_5/HWO-C$ and $K-V_2O_5/HWO-C$ recovered to 92% and 78% within 20 min,

1 respectively. Li et al [49] reported that the V_2O_5 -based catalysts exhibit a strong SO_2
 2 tolerance and weak alkali resistance performance. Hence the results of SCR stability
 3 test convince that effective alkali resistance of the K- V_2O_5 /HWO-C originates from
 4 the capture of HWO channels, and the slight interactions between alkalis and SO_2
 5 occurs owing to almost 0.71 % K^+ located on the HWO-C external surface. The SEM
 6 and NH_3 -TPD characterizations of the V_2O_5 /HWO-C and K- V_2O_5 /HWO-C catalysts
 7 after the SCR reaction have been supplied to explore the changes of morphology and
 8 acidity, as shown in Fig.S5 and Fig. S6, respectively. It can be found from Fig.S5 that
 9 the regular morphology is unchanged although the slight agglomeration on the
 10 catalyst surface, exhibiting the good resistance of SO_2 . After SO_2 -resistaing testing,
 11 the peak area becomes smaller and the temperature of peaks transform higher for the
 12 used V_2O_5 /HWO-C and K- V_2O_5 /HWO-C catalyst, indicating that the NH_3 adsorption
 13 might become relative weaker on the catalyst surface. A reasonable explanation is that
 14 the slight sulfated species occupy adsorption sites and disturb NH_3 adsorption, in
 15 agreement with the small activity reduction of the catalysts.



16
 17 **Fig. 12.** (a) SCR activity of the catalysts with the reaction condition: $[NH_3]=[NO]=300$ ppm,
 18 $[O_2]= 5$ vol.%; (b) Effect of SO_2 on the SCR duration tests under the V_2O_5 /HWO-C and
 19 K- V_2O_5 /HWO-C catalysts at 360 °C with the reaction condition: $[NH_3]=[NO]=400$ ppm, $[O_2]= 5$

1 vol.%, [SO₂]=500 ppm.

2 **Table 2.** The SCR activity over different catalysts under different reaction conditions.

Samples	Reaction gas mixture	GHSV (h ⁻¹)	Temperature (°C)	X _{NO} (%)	Ref.
V ₂ O ₅ /HWO	NO=NH ₃ =500 ppm, 3	200,000	350	92	[26]
K ₂ SO ₄ -V ₂ O ₅ /HWO	vol% O ₂ , 1,300 mg·m ⁻³	200,000	350	92	[26]
K ₂ SO ₄ -V ₂ O ₅ /WO ₃ -TiO ₂	SO ₂ , N ₂ balanced	200,000	350	<10	[26]
V ₂ O ₅ /HWO	NO=NH ₃ =1000 ppm, 3	80,000	350	90	[27]
V ₂ O ₅ /K _{in} HWO	vol% O ₂ , N ₂ balanced	80,000	350	~80	[27]
V ₂ O ₅ -S/CeO ₂	NO=NH ₃ =500 ppm,	100,000	350	~98	[30]
K-V ₂ O ₅ -S/CeO ₂	5 vol% O ₂ , N ₂ balanced	100,000	350	~95	[30]
K0.1-VWTi	NO=NH ₃ =500 ppm, 3	70,000	350	96	[41]
K1-VWTi	vol% O ₂ , N ₂ balanced	70,000	350	20	[41]
V ₂ O ₅ /TiO ₂	NO=NH ₃ =500 ppm, 5	8,000	400	95	[47]
K/V(1.3)-Imp-V ₂ O ₅ /TiO ₂	vol% O ₂ , 1,500 ppm SO ₂ ,	8,000	400	88	[47]
K/V(1.3)-Dif-V ₂ O ₅ /TiO ₂	5vol% H ₂ O, N ₂ balanced	8,000	400	80	[47]
V ₂ O ₅ /HWO-C	NH ₃ =NO=300 ppm,	170,000	360	97	
K-V ₂ O ₅ /HWO-C		170,000	360	83	
V ₂ O ₅ /HWO-O	O ₂ = 5 vol.%,	170,000	360	90	In this
K-V ₂ O ₅ /HWO-O	N ₂ balanced	170,000	360	74	work
V ₂ O ₅ /HWO-W		170,000	360	79	
K-V ₂ O ₅ /HWO-W		170,000	360	52	
V ₂ O ₅ /HWO-C	NH ₃ =NO=300 ppm,	170,000	360	91	
K-V ₂ O ₅ /HWO-C	O ₂ = 5 vol.%, SO ₂ =500	170,000	360	76	In this
V ₂ O ₅ /HWO-O	ppm, N ₂ balanced	170,000	360	84	work
K-V ₂ O ₅ /HWO-O		170,000	360	70	

3 To investigate the SCR reaction mechanism related to K⁺ poisoning and trapping,
4 samples for in situ IR analysis were pretreated under a N₂ flow of 100 mL/min with a
5 10 °C/min heating rate. Adsorption of 5 vol% NH₃/N₂ on V₂O₅/HWO-C (Fig. 13a)
6 leads to the formation of many NH₄⁺ species on the Brønsted acid sites at 1410 cm⁻¹
7 and the absorption of NH₃ on the Lewis acid sites at 1345 cm⁻¹ [51] [52]. In contrast, the
8 Brønsted adsorption on K-V₂O₅/HWO-C (Fig. 13b) nearly disappeared, although the
9 Lewis adsorption was obviously unchanged. The decrease in surface acid sites is
10 induced by the capture of K⁺ by HWO channels via the ion exchange pathway

1 (W-O-H + K⁺→W-O-K + H⁺), in agreement with the XRD and NH₃-TPD results.

2 With the increase of temperature from 50 to 500 °C, the 1345 cm⁻¹ peak of catalysts

3 became slightly stronger, which can be attributed to the activated NH₄⁺ species and

4 then transform to NH₃ on the catalyst surface. After pre-adsorption of 5 vol% NO +

5 air, absorbed NO (1630 cm⁻¹) and absorbed NO₂ (1600 cm⁻¹) are formed^{[53][54]}, and the

6 intensity of the peaks does not change for the V₂O₅ of V₂O₅/HWO-C and

7 K-V₂O₅/HWO-C (Fig. 13c-d). This behaviour confirms that the HWO channels can

8 effectively trap K⁺ and prevent K⁺ poisoning of V₂O₅. The bands at 1355 and

9 1300-1140 cm⁻¹ are attributed to the chelated nitrite and bidentate nitrate species,

10 respectively. In particular, the peak intensity at 1355 cm⁻¹ for K-V₂O₅/HWO-C is

11 higher than that for V₂O₅/HWO-C due to the occurrence of the K-O bond in the

12 catalyst, in agreement with XRD and Rietveld refinements results, and verified by the

13 literatures^{[24][26]}. With a temperature increase to 500 °C, the peaks of absorbed NO and

14 absorbed NO₂ decrease first, followed by the peaks of nitrite and nitrate species.

15 Similar spectra are observed for V₂O₅/HWO-C (Fig. 13e) and K-V₂O₅/HWO-C (Fig.

16 13f). The bands at 1513 and 1413 cm⁻¹ (NH₄⁺ species on the Brønsted acid sites),

17 1340 cm⁻¹ (NH₃ on the Lewis acid sites), 1626 cm⁻¹ (absorbed NO), and 1300-1140

18 cm⁻¹ (chelated nitrite and bidentate nitrate species) are observed. However, the band at

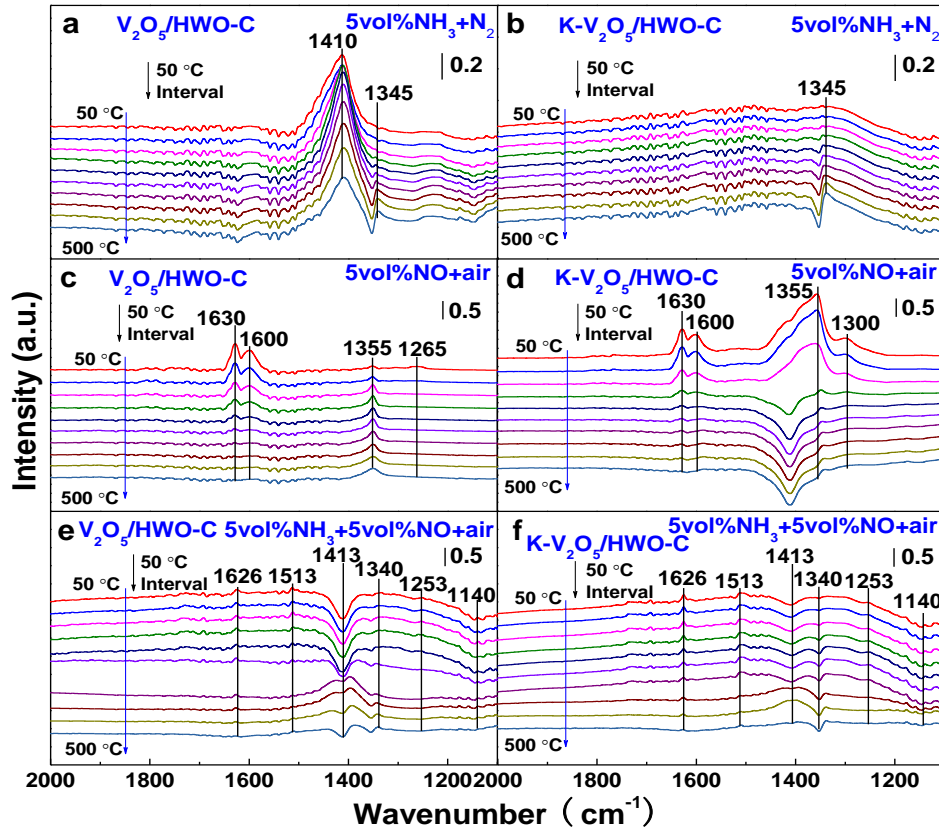
19 1413 cm⁻¹ of K-V₂O₅/HWO-C is weaker than that of V₂O₅/HWO-C under 5 vol%

20 NH₃ + 5 vol% NO + air pre-adsorption because of the slight K⁺ poisoning. With the

21 temperature increasing (50-500 °C), a series of NO_x species including NO_{abs}, NO_{2abs},

22 NO₂⁻ and NO₃⁻ are formed via NO+O₂ at the V₂O₅ sites, which react with the NH₄⁺

- 1 (Brønsted) and $\text{NH}_{3\text{abs}}$ (Lewis) groups of V_2O_5 and HWO sites to release N_2 and H_2O ,
- 2 following the Langmuir-Hinshelwood (L-H) mechanism.

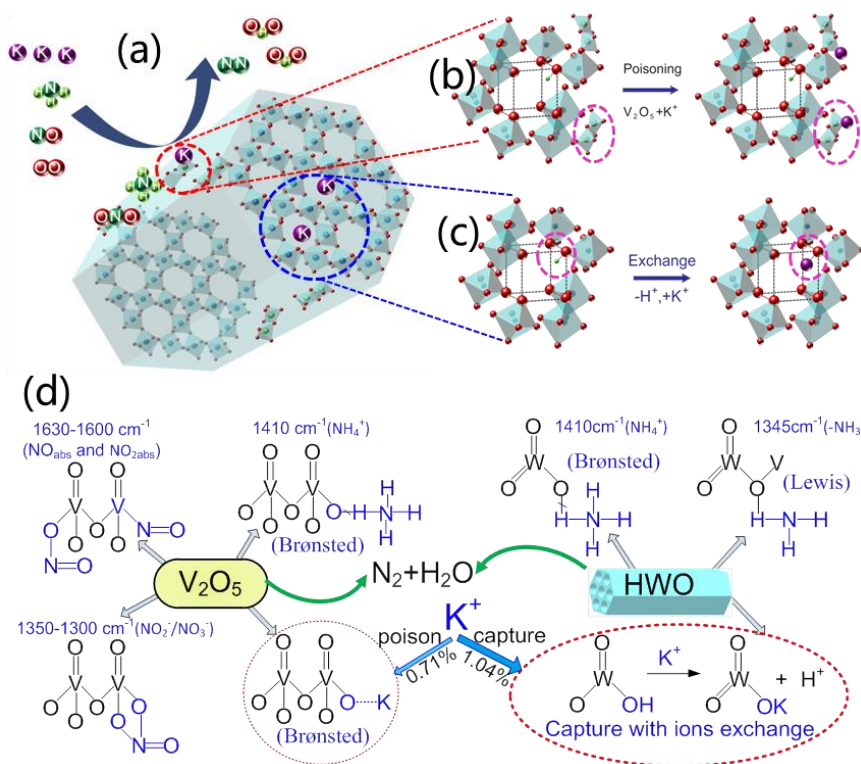


3
 4 **Fig. 13.** In situ IR spectra of $\text{V}_2\text{O}_5/\text{HWO-C}$ and $\text{K-V}_2\text{O}_5/\text{HWO-C}$ (50-500 °C) under different
 5 pre-adsorption conditions.

6 **3.4 K resistance mechanism for the SCR reaction**

7 According to the analysis above, the excellent activity obtained for
 8 $\text{V}_2\text{O}_5/\text{HWO-C}$ can be attributed to the well dispersed V_2O_5 on the smooth rod-shaped
 9 morphology of HWO and the abundant number of active oxygen atoms and acid sites
 10 on the catalyst surface. The proposed K resistance mechanism and detailed pathways
 11 of intermediates for the SCR reaction are shown in Fig. 14. Combined with the IR
 12 results, a series of NO_x species including NO_{abs} , $\text{NO}_{2\text{abs}}$, NO_2^- and NO_3^- are formed
 13 via $\text{NO} + \text{O}_2$ at the V_2O_5 sites, which react with the NH_4^+ (Brønsted) and $\text{NH}_{3\text{abs}}$ (Lewis)

1 groups of V_2O_5 and HWO to release N_2 and H_2O , following the L-H mechanism (Fig.
2 14a and Fig. 14d), verified by the Zhu et al [55]. Most K^+ (approximately 1.04 wt%)
3 can be effectively captured in the smooth rod-shaped HWO-C channels with via the
4 ion exchange pathway (Fig. 14c and Fig. 14d), because the K^+ ions inially react with
5 protons of HWO-C via ion exchange, and then are stably fixed at the alkali-trapping
6 sites via the coordination with the oxgen atoms of the cavities ($W-O-H + K^+ \rightarrow W-O-K$
7 $+ H^+$), concomitant with an energy saving [8][24]. Therefore, the $V_2O_5/HWO-C$ can
8 realize effective resistance of K poisoning via the coordination of the two sites: one is
9 the alkali capture sites of HWO, and the other is the active sites of V_2O_5 on the
10 catalyst. And the rest of K^+ ions (approximately 0.71 wt%) are located on the HWO-C
11 external surface via weak bonds to V_2O_5 , resulting in a decrease in the number of
12 Brønsted acid sites and some degree of alkali poisoning (Fig. 14b and Fig. 14d),
13 which is in agreement with the SCR activity results. In this case, the coordination of
14 the two sites is effectively realized for resisting K poisoning via the active sites of
15 V_2O_5 and the K capture sites of HWO-C channels on the K- $V_2O_5/HWO-C$ catalyst.



1

2 **Fig. 14.** Schematic model of the K- V_2O_5 /HWO-C catalyst: (a) SCR reaction mechanism with
 3 alkali metals, (b) slight alkali poisoning with V_2O_5 on the surface, (c) alkali resistance by HWO
 4 channel capture, and (d) detailed pathways of intermediates and forms of K^+ .

5 **4. Conclusions**

6 The V_2O_5 /HWO catalysts are synthesized using different pore-forming agents for
 7 the SCR of NO with NH_3 . The catalytic activity for SCR decreases in the order of
 8 V_2O_5 /HWO-C > V_2O_5 /HWO-O > V_2O_5 /HWO-W, which is due to the highly dispersed
 9 V_2O_5 , high specific surface area, abundant amounts of active oxygen, surface acidity,
 10 and smooth rod-shaped morphology of HWO in the V_2O_5 /HWO-C catalyst. The
 11 obtained results provide evidence that commercial bacterial cellulose achieves
 12 controllable synthesis to form catalysts with a regular morphology. The V_2O_5 /HWO-C
 13 catalyst exhibits a relative effective resistance of alkali and SO_2 . The NO_x
 14 intermediate species including NO_{abs} , NO_{2abs} , NO_2^- and NO_3^- are formed on the V_2O_5
 15 active sites and react with the NH_4^+ and NH_{3abs} groups of V_2O_5 and HWO, mainly

1 following the L-H mechanism during the SCR reaction. After being subjected to a K⁺
2 load, V₂O₅/HWO-C effectively resisted K poisoning via the coordination of the two
3 sites, where most of the K⁺ ions (1.04 wt%) can be effectively captured in the
4 HWO-C channels with K-O bond, and a slight amount of K⁺ (0.71 wt%) is located on
5 the HWO-C external surface and forms weak bonds with V₂O₅.

6 **Authorship contribution statement**

7 **Running Kang:** Catalyst prepared, Formal analysis, Experiments, Investigation,
8 Writing-original draft, Writing-review & editing. **Junyao He:** Experiments. **Feng Bin:**
9 Writing-review & editing, Constructive discussions. **Baojuan Dou:** Catalyst prepared
10 methods. **Qinglan Hao:** Catalyst prepared methods. **Xiaolin Wei:** Conceptualization,
11 Supervision. **Kwun Nam Hui:** Characterization methods and discussion. **Kwan San**
12 **Hui:** Writing-review & editing.

13 **Acknowledgements**

14 We sincerely thank Prof. Lv Gang (Tianjin University) for the help and
15 reasonable suggestions about SCR reaction mechanism. We gratefully acknowledge
16 the financial support from the National Natural Science Foundation of China (No.
17 51736010), and the Key Projects of Tianjin Natural Science Foundation
18 (19JCZDJC40100).

19 **Declaration of competing interest**

20 The authors declare that they have no conflict of interest.

21 **References**

22 [1] Y.J. Pan, B.X. Shen, L.J. Liu, Y. Yao, H.P. Gao, C. Liang, H.J. Xu. Develop high

- 1 efficient of NH₃-SCR catalysts with wide temperature range by ball-milled method.
2 Fuel. 282 (2020) 118834.
- 3 [2] J.K. Lai, I.E. Wachs. A perspective on the selective catalytic reduction (SCR) of
4 NO with NH₃ by supported V₂O₅-WO₃/TiO₂ Catalysts. ACS Catal. 8 (2018)
5 6537–6551.
- 6 [3] Y.Q. Hou, J.C. Wang, Q.Y. Li, Y.J. Liu, Y.R. Bai, Z.Q. Zeng, Z.G. Huang.
7 Environmental-friendly production of FeNbTi catalyst with significant enhancement
8 in SCR activity and SO₂ resistance for NO_x removal. Fuel. 285, (2021), 119133.
- 9 [4] I. Yusuke, K. Hiroe, H. Shinichi, K. Eiji, M. Keiichiro, Y. Kazuhiro, S. Norihito,
10 T.Y. Takashi, S. Kenichi, I. Satoshi, U. Wataru, H. Masatake, M. Toru. Bulk
11 tungsten-substituted vanadium oxide for lowtemperature NO_x removal in the
12 presence of water. Nat. Commun. 12(557) 2021 1-11.
- 13 [5] J.R. Strege, C.J. Zygarlicke, B.C. Folkedahl, D.P. McCollor. SCR deactivation in a
14 full-scale cofire-utility boiler. Fuel. 87 (7) (2008) 1341–1347.
- 15 [6] D. Nicosia, I. Czekaj, O. Krocher. Chemical deactivation of V₂O₅/WO₃-TiO₂ SCR
16 catalysts by additives and impurities from fuels lubrication oils and urea solution
17 Characterization study of the effect of alkali and alkaline earth metals. Appl. Catal., B:
18 Environ. 77 (2008) 228-236.
- 19 [7] S.L. Zhang, Q. Zhong. Surface characterization studies on the interaction of
20 V₂O₅-WO₃/TiO₂ catalyst for low temperature SCR of NO with NH₃. J. Solid. State.
21 Chem. 221 (2015) 49–56.
- 22 [8] Z.W. Huang, X. Gu, W. Wen, P.P. Hu, M. Makkee, H. Lin, F. Kapteijn, X.F. Tang.

1 A “smart” hollandite deNO_x catalyst: self-protection against alkali poisoning. *Angew.*
2 *Chem. Int. Ed.* 320(52) (2013) 660–664.

3 [9] X.X. Wang, Q.L. Cong, L. Chen, Y. Shi, Y. Shi, S.J. Li, W. Li. The alkali
4 resistance of CuNbTi catalyst for selective reduction of NO by NH₃: A comparative
5 investigation with VWTi catalyst. *Appl. Catal. B: Environ.* 246 (2019) 166–179.

6 [10] Q. Li, S. Chen, Z. Liu, Q. Liu. Combined effect of KCl and SO₂ on the selective
7 catalytic reduction of NO by NH₃ over V₂O₅/TiO₂ catalyst. *Appl. Catal. B. Environ.*
8 164 (2015) 475–482.

9 [11] S.X. Cai, T.Y. Xu, P.L. Wang, L.P. Han, S. Impeng, Y. Li, T.T. Yan, G.R. Chen,
10 L.Y. Shi, D.S. Zhang. Self-Protected CeO₂–SnO₂@SO₄²⁻/TiO₂ Catalysts with
11 Extraordinary Resistance to Alkali and Heavy Metals for NO_x Reduction. *Environ Sci*
12 *Technol*, 54(19), 2020, 12752-12760.

13 [12] L.J. Yan, Y.Y. Ji, P.L. Wang, C. Feng, L.P. Han, H.R. Li, T.T. Yan, L.Y. Shi, D.S.
14 Zhang. Alkali and Phosphorus Resistant Zeolite-like Catalysts for NO_x Reduction by
15 NH₃. *Environ Sci Technol*, 54(14), 2020, 9132-9141.

16 [13] P.L. Wang, L.J Yan, Y.D. Gu, S. Kuboon, H.R. Li, T.T. Yan, L.Y. Shi, D.S. Zhang.
17 Poisoning-Resistant NO_x Reduction in the Presence of Alkaline and Heavy Metals
18 over H-SAPO-34-Supported Ce-Promoted Cu-Based Catalysts. *Environ Sci Technol*,
19 54 (10) 2020, 6396-6405.

20 [14] J. Yang, W. Tang, X. Liu, C. Chao, J. Liu, D. Sun. Bacterial cellulose-assisted
21 hydrothermal synthesis and catalytic performance of La₂CuO₄ nanofiber for methanol
22 steam reforming, *In. J Hydrogen. Energ.* 38 (2013) 10813–10818.

- 1 [15] J. K. Lai, I. E. Wachs. A Perspective on the Selective Catalytic Reduction (SCR)
2 of NO with NH₃ by Supported V₂O₅-WO₃/TiO₂ Catalysts. ACS Catal. 8 (2018)
3 6537–6551.
- 4 [16] X. Wu, W. Yu, Z. Si, D. Weng. Chemical deactivation of V₂O₅-WO₃/TiO₂ SCR
5 catalyst by combined effect of potassium and chloride. Front. Environ. Sci. Eng. 7
6 (2013) 420–427.
- 7 [17] Z.H. Lian, Y.J. Li, W.P. Shan, H. He. Recent progress on improving
8 low-temperature activity of vanadia-based catalysts for the selective catalytic
9 reduction of NO_x with ammonia. Catalysts. 10(1421) 2020 1-19.
- 10 [18] Z.H. Lian, H. Deng, S.H. Xin, W.P. Shan, Q. Wang, J. Xu, H. He. Significant
11 promotion effect of rutile phase on V₂O₅/TiO₂ catalyst for NH₃-SCR. Chem.
12 Commun., 2020, DOI: 10.1039/D0CC05938B.
- 13 [19] L. Deng, X. Liu, P.Q. Cao, Y.G. Zhao, Y.B. Du, C.A. Wang, D.F. Che. A study on
14 deactivation of V₂O₅-WO₃-TiO₂ SCR catalyst by alkali metals during entrained-flow
15 combustion. J. Energy. Inst. 90 (2017) 743–751.
- 16 [20] M. Kong, Q.C. Liu, J. Zhou, L.J. Jiang, Y.M. Tian, J. Yang, S. Ren, J.L. Li. Effect
17 of different potassium species on the deactivation of V₂O₅-WO₃-TiO₂ SCR catalyst:
18 Comparison of K₂SO₄, KCl and K₂O. Chem. Eng. J. 348 (2018) 637-643.
- 19 [21] J. Li, Y. Peng, H. Chang, X. Li, J. C. Crittenden, J. Hao. Chemical poisoning and
20 regeneration of SCR catalysts for NO_x removal from stationary sources. Front.
21 Environ. Sci. Eng. 10 (2016) 413–427.
- 22 [22] Y. He, M. E. Ford, M. Zhu, Q. U. Tumuluri, L. Z. Wu, I. E. Wachs. Influence of

1 catalyst synthesis method on selective catalytic reduction (SCR) of NO by NH₃ with
2 V₂O₅-WO₃-TiO₂ catalysts. *Appl. Catal. B. Environ.* 193 (2016) 141–150.

3 [23] D. W. Kwon, K. H. Park, S. C. Hong. The influence on SCR activity of the
4 atomic structure of V₂O₅/TiO₂ catalysts prepared by a mechanochemical method.
5 *Appl. Catal. A: General.* 451 (2013) 227–235.

6 [24] P.P. Hu, Z.W. Huang, X. Gu, F. Xu, J. Gao, Y. Wang, Y. X. Chen, X. F. Tang.
7 Alkali-resistant mechanism of a hollandite DeNO_x catalyst. *Environ. Sci. Technol.* 49
8 (2015) 7042–7047.

9 [25] G.Y. Zhou, P. Maitarad, P.L. Wang, L.P. Han, T.T. Yan, H.R. Li, J.P. Zhang, L.Y.
10 Shi, D.S. Zhang. Alkali-Resistant NO_x Reduction over SCR Catalysts via Boosting
11 NH₃ Adsorption Rates by In Situ Constructing the Sacrificed Sites. *Environ Sci*
12 *Technol*, 54(20), 2020, 13314-13321.

13 [26] Z.W. Huang, H. Li, J.Y. Gao, X. Gu, L. Zheng, P.P. Hu, Y. Xin, J.X. Chen, Y.X.
14 Chen, Z.L. Zhang, J.M. Chen, X.F. Tang. Alkali- and sulfur-resistant tungsten-based
15 catalysts for NO_x emissions control. *Environ. Sci. Technol.* 49 (2015) 14460–14465.

16 [27] L. Zheng, M.J. Zhou, Z.W. Huang, Y.X. Chen, J.Y. Gao, Z. Ma, J.M.Chen, X.F.
17 Tang. Self-protection mechanism of hexagonal WO₃-based DeNO_x catalysts against
18 alkali poisoning. *Environ. Sci. Technol*, 50(19), 2016, 11951–11956.

19 [28] Q. Wan, L. Duan, J.H. Li, L. Chen, K.B. He, J.M. Hao, Deactivation performance
20 and mechanism of alkali (earth) metals on V₂O₅-WO₃/TiO₂ catalyst for oxidation of
21 gaseous elemental mercury in simulated coal-fired flue gas. *Catal Today.* 175 (2011)
22 189–195.

- 1 [29] S.W. Li, Y. Xu, Y.F. Chen, W.Z. Li, L.L. Lin, M.Z. Li, Y.C. Deng, X.P. Wang,
2 B.H. Ge, C. Yang, S.Y. Yao, J.L. Xie, Y.W. Li, X. Liu, D. Ma. Tuning the selectivity of
3 catalytic carbon dioxide hydrogenation over Iridium/Cerium oxide catalysts with a
4 strong metal-support interaction. *Angew. Chem. Int. Ed.* 56 (2017) 10761–10765.
- 5 [30] K.W. Zha, L. Kang, C. Feng, L.P. Han, H.R. Li, T.T. Yan, P. Maitarad, L.Y. Shi,
6 D.S. Zhang, Improved NO_x reduction in the presence of alkali metals by using
7 hollandite Mn-Ti oxides promoted Cu-SAPO-34 catalysts, *Environ. Sci.: Nano.* 5
8 (2018) 1408–1419.
- 9 [31] R.D. Shannon. Revised effective ionic radii and systematic studies of interatomic
10 distances in halides and chalcogenides, *Acta. Crystallogr. A.* 32 (1976) 751–767.
- 11 [32] L. Chen, S.W. Lam, Q.H. Zeng, R. Amal, A.B. Yu, Effect of cation intercalation
12 on the growth of hexagonal WO₃ nanorods. *J. Phys. Chem. C*, 116(21) (2012)
13 11722–11727.
- 14 [33] N. Zhu, W.P. Shan, Z.H. Lian, Y. Zhang, K. Liu, H. He. A superior Fe-V-Ti
15 catalyst with high activity and SO₂ resistance for the selective catalytic reduction of
16 NO_x with NH₃. *J. Hazard. Mater.* 382 (2020) doi: 10.1016/j.jhazmat.2019.120970.
- 17 [34] S.L. Zhang, Q. Zhong, Surface characterization studies on the interaction of
18 V₂O₅–WO₃/TiO₂ catalyst for low temperature SCR of NO with NH₃. *J. Solid State*
19 *Chem.* 221 (2015) 49–56.
- 20 [35] S.L. Zhang, Q. Zhong. Promotional effect of WO₃ on O²⁻ over V₂O₅/TiO₂
21 catalyst for selective catalytic reduction of NO with NH₃. *J. Mol. Catal. A-Chem.*, 373
22 (2013), 108-113.

- 1 [36] J.P. Chen, R.T. Yang, Role of WO_3 in mixed $\text{V}_2\text{O}_5\text{-WO}_3/\text{TiO}_2$ catalysts for
2 selective catalytic reduction of nitric oxide with ammonia, *Appl. Catal. A. Gen.* 80
3 (1992) 135–148.
- 4 [37] J.W. Shi, Y. Wang, R.B. Duan, C. Gao, B.R. Wang, C. He, C.M. Niu. The
5 synergistic effects between Ce and Cu in $\text{Cu}_y\text{Ce}_{1-y}\text{W}_5\text{O}_x$ catalysts for enhanced
6 $\text{NH}_3\text{-SCR}$ of NO_x and SO_2 tolerance. *Catal. Sci. Technol.*, 9 (2019) 718-730]
- 7 [38] D. Wang, Y. Peng, S.C. Xiong, B. Li, L.N. Gan, C.M. Lu, J.J. Chen, Y.L. Ma, J.H.
8 Li. De-reducibility mechanism of titanium on maghemite catalysts for the SCR
9 reaction: An in situ DRIFTS and quantitative kinetics study. *Appl. Catal. B. Environ.*
10 221 (2018) 556–564.
- 11 [39] J.Q. Huang, Z.H. Teng, R.N. Kang, F. Bin, X.L. Wei, Q.L. Hao, K.N. Hui, K.S.
12 Hui, B.J. Dou. Study on activity, stability limit and reaction mechanism of CO
13 self-sustained combustion over the LaMnO_3 , $\text{La}_{0.9}\text{Ce}_{0.1}\text{MnO}_3$ and $\text{La}_{0.9}\text{Sr}_{0.1}\text{MnO}_3$
14 perovskite catalysts using sugar agent. *Fuel*, 292 (2021), 120289.
- 15 [40] M.A. Reiche, M. Maciejewski, A. Baiker, Characterization by temperature
16 programmed reduction. *Catal. Today* 56 (2000) 347–355.
- 17 [41] L. Chen, J.H. Li, M.F. Ge. The poisoning effect of alkali metals doping over nano
18 $\text{V}_2\text{O}_5\text{-WO}_3/\text{TiO}_2$ catalysts on selective catalytic reduction of NO_x by NH_3 . *Chem. Eng.*
19 *J.*, 170 (2011), 531–537.
- 20 [42] F. Bin, C. Song, G. Lv, J. Song, X. Cao, H. Pang, K. Wang. Structural
21 characterization and selective catalytic reduction of nitrogen oxides with ammonia: a
22 comparison between Co/ZSM-5 and Co/SBA-15 . *J. Phys. Chem. C.* 116 (2012)
23 26262–26274.
- 24 [43] F. Bin, C. Song, G. Lv, J. Song, S. Wu, X. Li. Selective catalytic reduction of

1 nitric oxide with ammonia over zirconium-doped copper/ZSM-5 catalysts. Appl.
2 Catal. B. Environ. 150–151 (2014) 532– 543.

3 [44] L. Zhong, W. Cai, Y. Yu, Q. Zhong. Insights into synergistic effect of chromium
4 oxides and ceria supported on Ti-PILC for NO oxidation and their surface species
5 study. Appl. Sur. Sci. 325 (2015) 52–63.

6 [45] N. Y. Topsøe, H. Topsøe, J. A. Dumesic. Vanadia/titania catalysts for selective
7 catalytic reduction (SCR) of nitric oxide by ammonia. J. Catal. 151 (1995) 226-240.

8 [46] L. Lietti. Reactivity of V₂O₅-WO₃/TiO₂ de-NO_(x) catalysts by transient methods.
9 Appl. Catal. B. Environ. 10 (1996) 281–297.

10 [47] T.Y. Lei, Q.C. Li, S.F. Chen, Z.Y. Liu, Q.Y. Liu. KCl-induced deactivation of
11 V₂O₅-WO₃/TiO₂ catalyst during selective catalytic reduction of NO by NH₃:
12 Comparison of poisoning methods. Chem. Eng. J, 296 (2016) 1–10.

13 [48] R.T. Guo, S.X. Wang, W.G. Pan, A.Y. Li, P. Sun, A.M. Liu, X. Sun, S.W. Liu,
14 Different poisoning effects of K and Mg on the Mn/TiO₂ catalyst for selective
15 catalytic reduction of NO_x with NH₃: A Mechanistic Study, J. Liu. J. Phys. Chem. C.
16 121 (2017) 7881–7891.

17 [49] Q. Li, S.Chen, Z. Liu, Q. Liu. Combined effect of KCl and SO₂ on the selective
18 catalytic reduction of NO by NH₃ over V₂O₅/TiO₂ catalyst. Appl. Catal. B. Environ.
19 164 (2015), 475-482.

20 [50] J. Chen, R. T. Yang. Mechanism of Poisoning of the V₂O₅/TiO₂ Catalyst for the
21 Reduction of NO by NH₃. J. Catal. 125 (1990), 411-420.

22 [51] W.S. Hu, Y.H. Zhang, S.J. Liu, C.H. Zheng, Xiang Gao, I. Nova, E. Tronconi,
23 Improvement in activity and alkali resistance of a novel V-Ce(SO₄)₂/Ti catalyst for

1 selective catalytic reduction of NO with NH₃, *Appl. Catal. B: Environ.* 206 (2017)
2 449–460.

3 [52] S. B. Rasmussen, R. Portela, P. Bazin, P. Ávila, M. A. Bañares, Daturi, M.
4 Transient operando study on the NH₃/NH₄⁺ interplay in V-SCR monolithic catalysts.
5 *Appl. Catal. B: Environ.* 224 (2018) 109–115.

6 [53] A. Marberger, D. Ferri, M. Elsener, O. Krocher. The significance of lewis acid
7 sites for the selective catalytic reduction of nitric oxide on vanadium-based catalysts.
8 *Angew. Chem., Int. Ed.* 55 (2016) 11989–11994.

9 [54] K. Hadjiivanov, P. Concepcion. Analysis of oxidation states of vanadium in
10 vanadia–titania catalysts by the IR spectra of adsorbed NO. *Top. Catal.* 12 (2000)
11 123–130.

12 [55] M. Zhu, J.K. Lai, U. Tumuluri, M.E. Ford, Z. Wu, I.E. Wachs. Reaction pathways
13 and kinetics for selective catalytic reduction (SCR) of acidic NO_x emissions from
14 power plants with NH₃. *ACS Catal.* 7 (2017) 8358–8361.
15
16